Available online at www.synsint.com

Synthesis and Sintering

ISSN 2564-0186 (Print), **ISSN** 2564-0194 (Online)

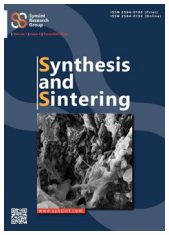

Research article

Synthesis and characterization of ZnS and Ag-ZnS nanoparticles for photocatalytic degradation of aqueous pollutants

Amir Hossein Afzali [a], Arshia Seddiqi [a], Zahra Akbari [a], Maryam Hajiebrahimi [a], Sanaz Alamdari [b], Omid Mirzaee [a,*]

[a] *Faculty of Materials and Metallurgical Engineering, Semnan University, Semnan, Iran*

[b] *Department of Nanotechnology, Faculty of New Sciences and Technologies, Semnan University, Semnan, Iran*

ABSTRACT

Photocatalytic degradation has drawn much interest recently as a substitute technique for eliminating environmental contaminants from the aqueous phase. In this study, pure and Ag-doped zinc sulfide (ZnS) nanoparticles were synthesized for the photocatalytic degradation of methylene blue (MB) under UVA light irradiation using a simple chemical co-precipitation method. The nanopowders' structural, optical, morphological, and chemical properties were characterized using XRD, FTIR, UV-Vis, and FESEM techniques. XRD analysis confirmed the hexagonal crystal structure of the nanoparticles, while FTIR identified stretching vibrations corresponding to O–H, C–H, C=O, C–N, and Zn–S bonds. The UV-Vis analysis revealed an optical band gap in the range of 5.2–5.4 eV. Photocatalytic performance tests under UVA light demonstrated that Ag doping significantly enhanced the photocatalytic efficiency of ZnS nanoparticles in degrading MB. Upon exposure to UVA light, the synthesized Ag-ZnS nanoparticles achieved impressive decolorization efficiency within 25 minutes, compared to 35 minutes for pure ZnS. The findings indicate that Ag-ZnS is a highly promising photocatalyst for the efficient removal of aqueous pollutants, including methylene blue dye.

KEYWORDS

Zinc sulfide
Ag dopant
Co-precipitation
Nanoparticles
Photocatalytic activity

OPEN ACCESS

1. Introduction

The global freshwater crisis has been identified as a significant challenge, with water stress expected to impact nearly every region worldwide shortly. Pollution, particularly in water contamination, disrupts ecosystem balance and leads to a host of water-related illnesses. These illnesses range from infectious diseases like waterborne and vector-borne infections to non-communicable conditions caused by exposure to chemically polluted water, including anemia, migraines, and cancer risks. Addressing water pollution is essential for safeguarding human health and ecosystems. Photocatalytic technologies have emerged as a highly effective solution for mitigating environmental degradation caused by pollutants [1–3]. Among these, semiconductor photocatalysis stands out as a promising approach for degrading organic contaminants in water. Zinc sulfide (ZnS) photocatalysts, in particular, have garnered attention for their ability to reduce the impact of hazardous waste. This study focuses on the photocatalytic degradation of methylene blue (MB), a synthetic dye commonly used in industries such as textiles and leather that poses significant environmental and health risks when released into water bodies without proper treatment [4–10].

* Corresponding author. *E-mail address:* o_mirzaee@semnan.ac.ir (O. Mirzaee)

Received 31 October 2024; Received in revised form 30 November 2024; Accepted 2 December 2024.

https://doi.org/10.53063/synsint.2024.44258

The advantages of this method include its high decomposition efficiency, rapid pollutant degradation, and improved absorption due to the nanoparticles' high surface-to-volume ratio. Under UV or visible light, photons with energy equal to or greater than the semiconductor's band gap excite electron-hole (e^-/h^+) pairs. These pairs generate reactive oxygen species (ROS) like superoxide and hydroxyl radicals on the photocatalyst's surface. These ROSs attack and degrade organic pollutants near the catalyst, breaking them down into harmless byproducts such as water and carbon dioxide [11–15]. Although ZnS is a widely studied semiconductor photocatalyst, its high band gap energy (3.54 eV) and rapid e^-/h^+ recombination limit its efficiency. Strategies to overcome these limitations include doping with metallic or non-metallic substances, coupling semiconductors, using appropriate supports, and synthesizing ZnS as nanoparticles to improve activity and reduce recombination rates [4, 8, 10, 13, 16]. Unlike commonly explored metal oxides requiring high-temperature calcination, metal sulfides like ZnS can be synthesized under milder conditions, making them environmentally advantageous. Moreover, their low water solubility prevents the leaching of metal ions, reducing the risk of secondary pollution [16–18].

The co-precipitation synthesis approach, which is more straightforward and efficient than other synthesis techniques, is used to manufacture zinc sulfide photocatalysis. The co-precipitation method is often selected for the synthesis of materials due to its simplicity, cost-effectiveness, and efficiency in controlling the chemical composition of the final product. This method allows for precise tuning of stoichiometry and offers a straightforward approach for scaling up material production without the need for expensive or complex equipment, unlike hydrothermal or sol-gel techniques. While the hydrothermal method requires high temperature and pressure conditions, and the sol-gel process involves additional steps such as gelation and thermal treatment, co-precipitation can be conducted at milder conditions, reducing processing time and costs. Additionally, co-precipitation provides better control over the particle size and morphology of the synthesized materials, which is crucial for various applications in catalysis, energy storage, and environmental remediation. This method is particularly advantageous when large quantities of homogeneous nanoparticles or composite materials are required. Furthermore, its adaptability to a wide range of precursor materials makes it a versatile and widely applicable technique in both research and industrial settings. Compared to hydrothermal and sol-gel methods, co-precipitation's efficiency, scalability, and simplicity offer significant advantages, particularly when large-scale production and economic feasibility are essential. Doping has emerged as a key strategy for enhancing the photocatalytic efficiency of ZnS nanostructures by tailoring their electronic and structural properties [19–26]. For instance, doping with transition metals such as Fe, Ni, Mn, and Co modifies the band gap, improving responsiveness to visible light, while also enhancing light absorption and electron transport. These modifications are critical for dye degradation applications [27–29]. Dixit et al. reported an impressive photocatalytic efficiency of 93.06% for the degradation of RhB dye at an optimal Fe doping concentration of 5%. This significant enhancement is primarily attributed to the role of Fe ions in facilitating the capture and transport of charge carriers, effectively minimizing recombination losses and thereby improving the overall photocatalytic performance [27]. In another study, Jothibas et al. [28] demonstrated that Ni doping substantially enhances the performance of ZnS. It significantly boosts photocatalytic activity, optimizes the band gap energy, as indicated by a blue shift with varying Ni concentrations, and stabilizes the cubic crystal structure, thereby improving structural integrity. These modifications ensure the material's reliability and effectiveness for long-term applications, particularly in environmental remediation and optoelectronic devices [28]. In other research, Rajabi et al. [29] revealed that incorporating 5% transition metal ions (Mn^{2+}, Co^{2+}, and Ni^{2+}) into ZnS quantum dots significantly enhances their photocatalytic activity, particularly in the decolorization of methyl violet dye. This enhancement is achieved through modifications to surface states, energy levels, and other intrinsic material properties, which collectively boost photoreactivity. Additionally, these dopants mitigate undesirable surface reactions, localize excitations, and facilitate efficient photon energy transfer [29].

The co-precipitation synthesis technique was used in this work to create ZnS and Ag-ZnS nanoparticles. Based on the structural and morphological analysis, ZnS nanoparticles were effectively synthesized. More significantly, the resulting Ag-ZnS nanoparticles exhibit better photocatalytic activity and effective dye degradation (e.g., methylene blue), which has a broad range of uses in water treatment.

2. Materials and Methods

2.1. Materials

All chemical precursors were employed without further purification because they were of analytical purity. Zinc acetate dehydrate ($Zn(CH_3COO)_2.2H_2O$) with a purity of 99.9%, sodium sulfide (Na_2S) with a purity of 99.9%, and silver nitrate ($AgNO_3$) as a dopant was all bought from Sigma-Aldrich, and ethanol and deionized water was used to produce aqueous solutions.

2.2. Synthesis of zinc sulfide (ZnS)

Synthesis of ZnS NPs was accomplished using the co-precipitation technique. First, 5 g of zinc acetate dihydrate and 3 g of sodium sulfide were each dissolved separately in 50 ml of deionized water, resulting in concentrations of approximately 0.4 M for zinc acetate dihydrate and 0.7 M for sodium sulfide. The solutions were then stirred individually using a magnetic stirrer for 30 min. The zinc acetate solution was then gradually added to the sodium sulfide solution using a separating funnel. A white precipitate was produced by mixing a room-temperature sodium sulfide solution with a zinc acetate solution. The solution was then supplemented with 2 at% silver nitrate and agitated for another 30 min after being swirled for 1 h. Next, the precipitate underwent washing, centrifugation, and drying at 80 °C for 24 hours. Finally, zinc sulfide powder was produced by calcining the final sample for 1 h at 800 °C. Fig. 1 shows a simplified flow diagram of the synthesis process.

2.3. Characterization

XRD analysis (Bruker D8-Advance) was employed to identify the crystal structure of the nanopowder using Cu Kα radiation (λ = 1.5406 Å) in which powders were scanned from 20 ° to 80 °. Field emission scanning electron microscopy (FESEM-TESCAN), operating at an acceleration voltage of 15 kV, was employed to study the morphology and size analysis of nanopowders. Vibrational modes and functional groups were examined using FTIR spectra (Perkin–Elmer

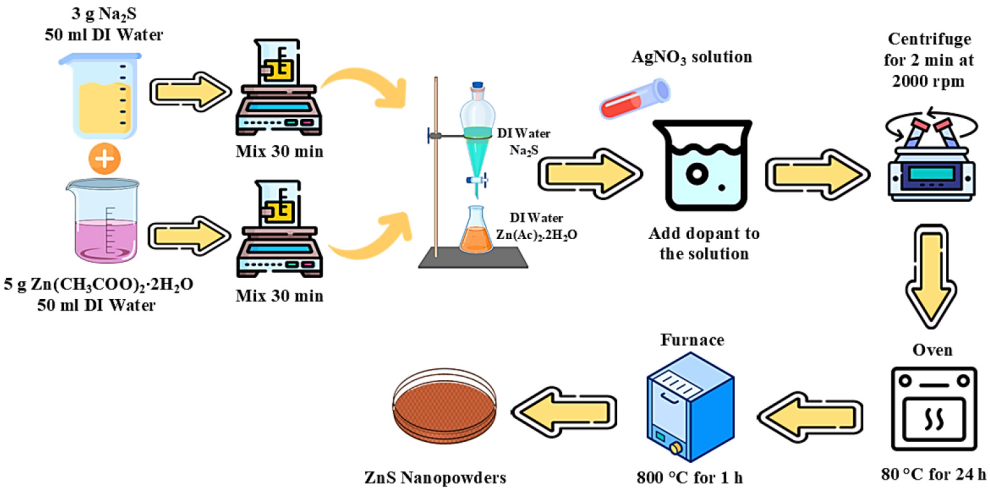

Fig. 1. Synthesis of zinc sulfide nanopowders.

Model 1800-USA). UV–visible spectrophotometer (Perkin-Elmer LS-5) in the 200 nm to 400 nm spectral range was employed to investigate the transmission spectrum of ZnS nanoparticles.

3. Results and discussion

3.1. X-ray diffraction (XRD)

The diagram of ZnS and ZnS doped with silver (Ag-ZnS) X-ray diffraction (XRD) patterns is shown in Fig. 2. In the hexagonal wurtzite structure of ZnS, the peaks are indexed to the (100), (002), (101), (102), (110), (103), (200), (112), (201), (202), (203), and (210) planes. Reference card (JCPDS card no. 96-901-3413) shows a typical diffraction pattern with crystal lattice constants of a = 0.382 and c = 0.626, which matches this structure. According to Fig. 2, there is a clear change in the peak locations and intensity after the Ag ion doped into the ZnS lattice, suggesting that the lattice has been distorted. This change in peaks indicates that the doping process was effective and that Ag-ZnS nanoparticles were formed. The introduction of Ag ions into the ZnS lattice increases peak intensity, indicating enhanced crystallinity and the successful substitution of Ag ions within the ZnS lattice. The XRD pattern of Ag-doped ZnS shows a slight shift of the (100) and (101) peaks towards higher 2θ angles. This shift can be attributed to lattice contraction caused by the larger ionic radius of Ag^+ (1.29 Å) compared to Zn^{2+} (0.74 Å). This observation confirms the successful substitution of Ag^+ for Zn^{2+} in the ZnS crystal lattice without altering its hexagonal structure [17].

Scherrer's equation (Eq. 1) was employed to calculate the average crystallite size of the synthesized samples. This technique comprises the use of the X-ray diffraction angle (θ) and the width at half the height of the principal peak (β) to determine the average crystal size based on three peaks with the greatest intensities. To determine the size of the crystallite, denoted by the letter 'D', in nanometers, the formula that follows should be used, where 'K' represents the shape factor of the normal crystallite, which is generally 0.9 [17, 30]:

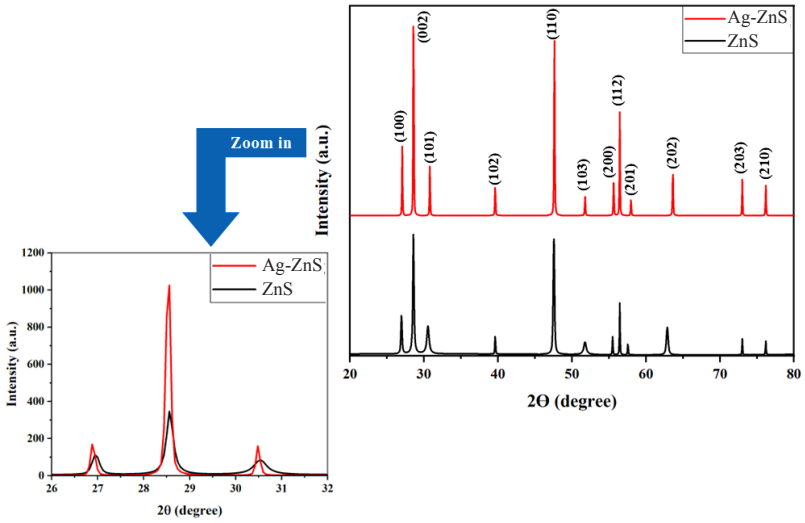

Fig. 2. XRD spectra of pure ZnS and Ag-doped ZnS and comparison of spectra.

Table 1. Determination of crystallite size of samples.

Sample	2θ (°)	FWHM (full width at half maximum)	D (nm)
ZnS	28.5646	0.1771	38.56
	47.5511	0.2362	
	56.3899	0.2952	
Ag-ZnS	28.2331	0.2362	32.95
	47.5010	0.2952	
	56.5373	0.2952	

$$D = \frac{K\lambda}{\beta \cos\theta} \quad (1)$$

The average particle size for pure ZnS was evaluated to be 38.56 nm, whereas for Ag-ZnS nanoparticles samples it was 32.95 nm, and other structural parameters of samples are reported in Table 1 [13, 17]. When Ag ions are doped into the ZnS lattice, they typically result in smaller crystallite sizes due to the difference in ionic radii. These changes can be attributed to lattice contraction caused by the larger ionic radius of Ag^{+} (1.29 Å) compared to Zn^{2+} (0.74 Å).

3.2. Fourier transform infrared spectroscopy (FTIR)

Multiple distinct vibrational modes, corresponding to different functional groups and bonding structures, are seen in the Fourier transform infrared spectra of both ZnS and Ag-doped ZnS (Ag-ZnS) in Fig. 3 and also, the frequencies of all vibrational bands that were analyzed are presented in Fig. 3. The FTIR spectrum of ZnS shows that the stretching vibrations of O–H, C–H hydrocarbon, C=O, C–N, and Zn–S are at 3450 cm^{-1}, 2900 cm^{-1}, 1637 cm^{-1}, 1095 cm^{-1}, and 624 cm^{-1}, respectively. The presence of these peaks indicates various functional groups and contaminants in the ZnS sample [8, 9, 16]. Compared to the undoped ZnS, the FTIR spectrum of the Ag-doped ZnS illustrates noticeable changes in peak intensities and shifts. The little change in the O–H stretching vibration peak from 3450 cm^{-1} in ZnS to 3429 cm^{-1} in Ag-ZnS indicates that the hydrogen bonding environment has changed because of the addition of Ag ions. A slight shift in the C=O stretching peak from 1637 cm^{-1} to 1640 cm^{-1} indicates that the carbonyl groups within the structure are interacting with Ag ions. The bonding environment of nitrogen-containing groups changes as a result of the doping procedure, as the C–N stretching vibration peak moves from 1095 cm^{-1} in ZnS to 1115 cm^{-1} at Ag-ZnS.

The C–H hydrocarbon stretching peak at 2900 cm^{-1} does not occur in the Ag-ZnS sample, which is a notable discrepancy between the spectra. The fact that these hydrocarbon contaminants were not present in the initial ZnS sample implies that the doping procedure with Ag ions may have eliminated or changed them. Enhanced catalytic activity or interactions that promote the decomposition of organic contaminants might be the reason why the addition of Ag ions could make it easier to break down or remove these hydrocarbon groups [10, 13, 17]. By comparing the two FTIR spectra, it is clear that the vibrational modes and bonding structures inside the ZnS material undergo substantial modifications due to Ag doping.

Changes in peak locations and the loss of the C–H hydrocarbon peak demonstrate how Ag ions affect ZnS's chemical environment and structural characteristics. These modifications are caused by variations in the chemical composition and bonding structure brought about by Ag ion interactions with different functional groups. Alterations in the FTIR spectra confirm the XRD-observed structural and compositional alterations, adding further proof that Ag doping affects the ZnS nanoparticles' characteristics [17].

3.3. FESEM images

The morphological properties and particle size distributions of pure ZnS and Ag-doped ZnS are shown in Fig. 4. Fig. 4a, the FESEM picture of the ZnS sample, reveals a very even dispersion of particles ranging in shape from spherical to hexagonal. The image histogram of particle size distribution shows that most particles are around 150 nm on average. The morphology indicates that the crystalline structures were well synthesized since there was little agglomeration. There don't seem to be any major flaws in the crystal development, as the surface is smooth [10, 17]. Fig. 4b shows that the Ag-doped ZnS sample also contains particles with spherical and hexagonal forms in the FESEM picture. Yet, the histogram of particle sizes shows that the average size has dropped to around 125 nm. It is hypothesized that the inclusion of Ag ions leads to a reduction in particle size, resulting in the formation of nanoparticles that are smaller than before. The presence of Ag ions may cause lattice distortions and additional surface defects, as shown in

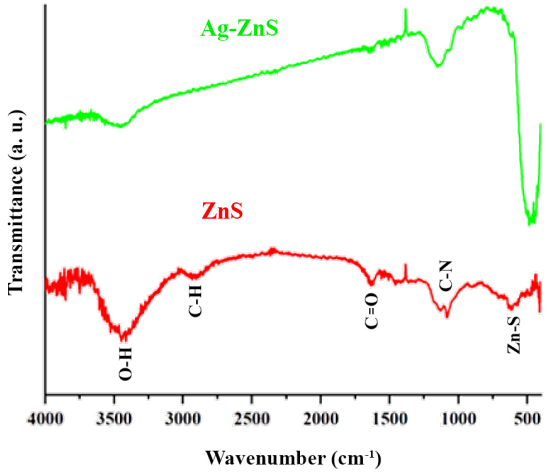

Fig. 3. FTIR spectra of pure ZnS and Ag-doped ZnS.

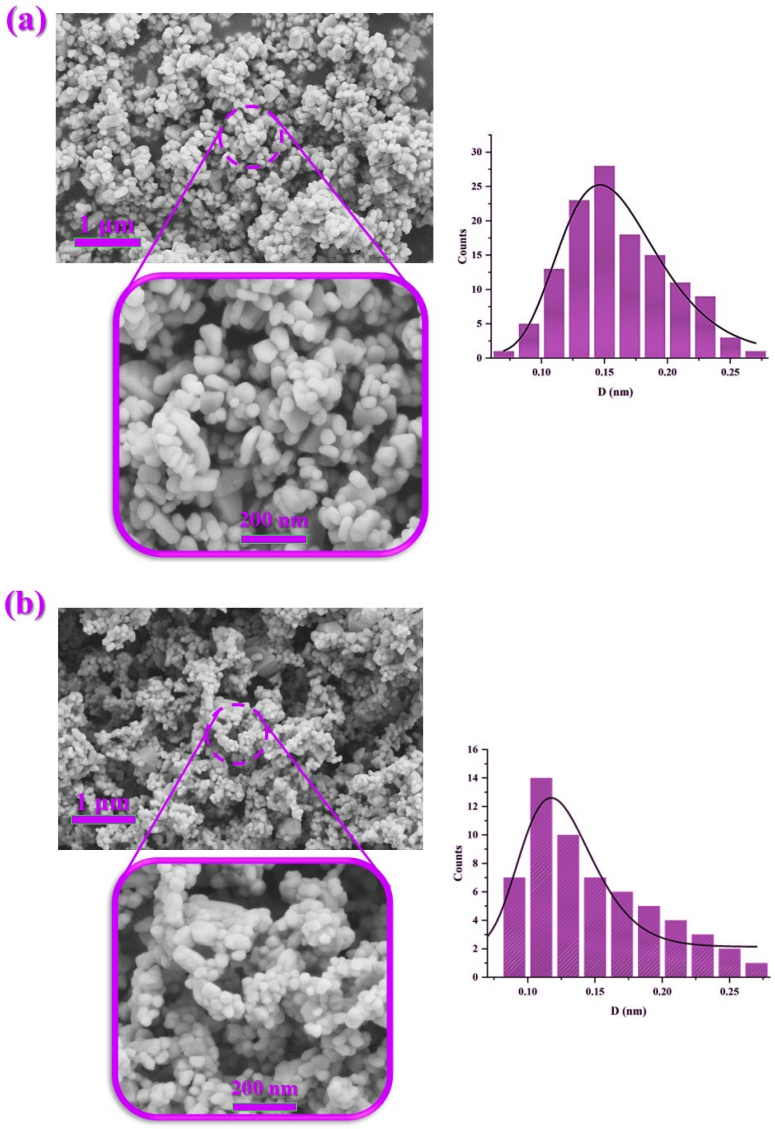

Fig. 4. FESEM images and particle size distributions of a) ZnS and b) Ag-ZnS nanopowders.

the significantly rougher surface morphology of Ag-ZnS nanoparticles compared to the pure ZnS sample [25, 26]. The FESEM study shows that Ag doping changes the structural parameters of ZnS nanoparticles, showing that Ag may change the shape and size of the particles, which is important for uses that need certain nanoparticle qualities.

3.4. UV–vis

In the UV technique, the absorption spectrum is measured in the ultraviolet region, allowing the determination of the electron spectrum of a substance through ultraviolet absorption spectroscopy. This process involves electron transfer due to the interaction of ultraviolet rays with the substance. Using Planck's equation ($\alpha hv=A(hv-Eg)^n$), the band gap characteristic of the synthesized nanoparticles was examined. UV absorption spectrum provided the wavelength of maximum absorption for the sample that is shown in Fig. 5a & b. The optical absorption edge for ZnS and Ag-ZnS was measured at 230 nm and 250 nm, respectively, with corresponding optical band gaps calculated as 5.2 eV and 5.4 eV [13, 17, 31, 32]. Based on these results, by doping Ag^+ ions, the optical band gap energy has increased. It is well-known that, because of quantum confinement effects, the optical band gap of semiconductor nanostructures is enhanced as the particle size decreases.

3.5. Photocatalytic activity

The photocatalytic performance of the ZnS and Ag-ZnS samples was evaluated by measuring the degradation rate of methylene blue dye when exposed to UVA light. To conduct this investigation, 0.005 grams of the synthesized sample were prepared with blue-colored solutions (C_0 = 0.020 g/l). These solutions were dissolved in neutral pH and placed in separate containers with an initial volume of 50 ml each, positioned 20 cm from the UV lamp. The solutions were stirred vigorously for 15 minutes before light irradiation to achieve absorption/desorption equilibrium.

Once the UV lamp was turned on, stirring continued, and 5 ml samples were taken at 5-minute intervals from the mother solution for ZnS and

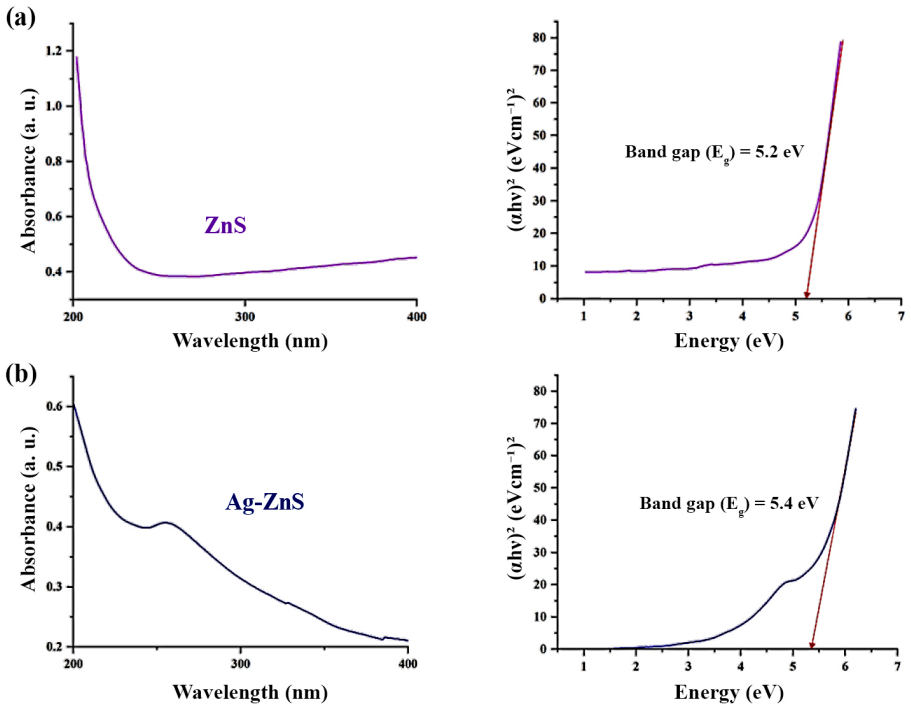

Fig. 5. UV–vis absorbance spectra band gap energies for a) pure ZnS and b) Ag-doped ZnS nanopowders.

Ag-ZnS. The samples were centrifuged at 5000 rpm to settle the photocatalyst nanoparticles. The UV absorption spectra of the methylene blue solution, catalyzed by the synthesized samples showed a decrease in absorption intensity with increasing reaction time. For ZnS, within 35 minutes, and for Ag-ZnS, within 25 minutes, the absorption intensity of methylene blue significantly decreased, indicating that both pure and dope samples effectively decomposed the organic dye in the solution (Fig. 6).

Important alterations in the absorption properties are noted with Ag doping. Ag-doped zinc sulfide has enhanced the photocatalytic efficiency of pure ZnS. Incorporating silver (Ag) into zinc sulfide (ZnS) significantly enhances its photocatalytic activity through various mechanisms. Silver nanoparticles improve light absorption via localized surface plasmon resonance (LSPR), enabling ZnS to utilize a broader light spectrum, particularly in the visible range. Ag also serves as an electron sink, capturing photoexcited electrons and reducing electron-hole recombination, which boosts photocatalytic efficiency. The formation of Ag-ZnS heterojunctions creates an electric field that further aids charge separation. Additionally, Ag increases the surface area available for catalytic reactions and can modify the electronic structure of ZnS, potentially reducing its band gap. These combined effects result in a marked improvement in the photocatalytic activity of ZnS, making it more effective for applications like environmental cleanup and hydrogen production.

Also, the performance results of the decolorization of methylene blue by the synthesized ZnS and Ag-ZnS samples are shown in Fig. 7. The pure ZnS shows 86% degradation efficiency after 35 min, while Ag-ZnS demonstrates 91% degradation efficiency in 25 minutes.

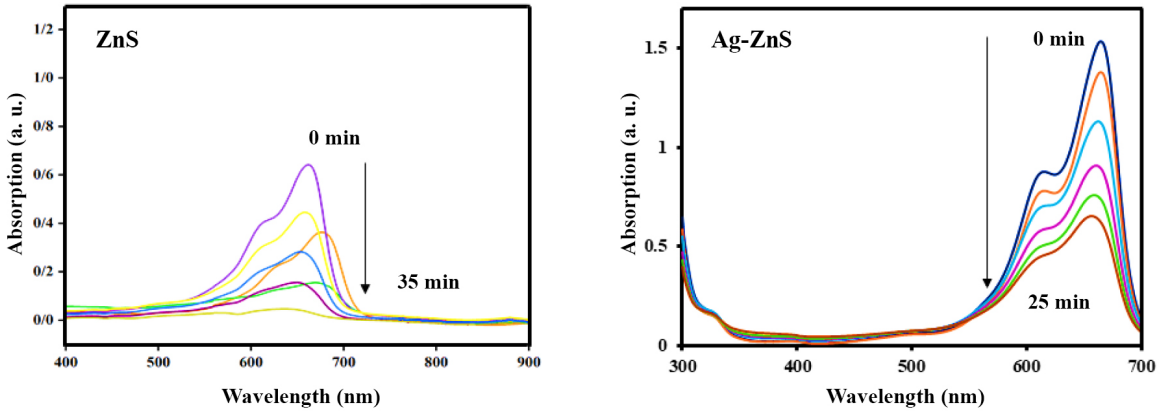

Fig. 6. UV–VIS absorption spectrum of methylene blue solution catalyzed by ZnS and Ag-ZnS.

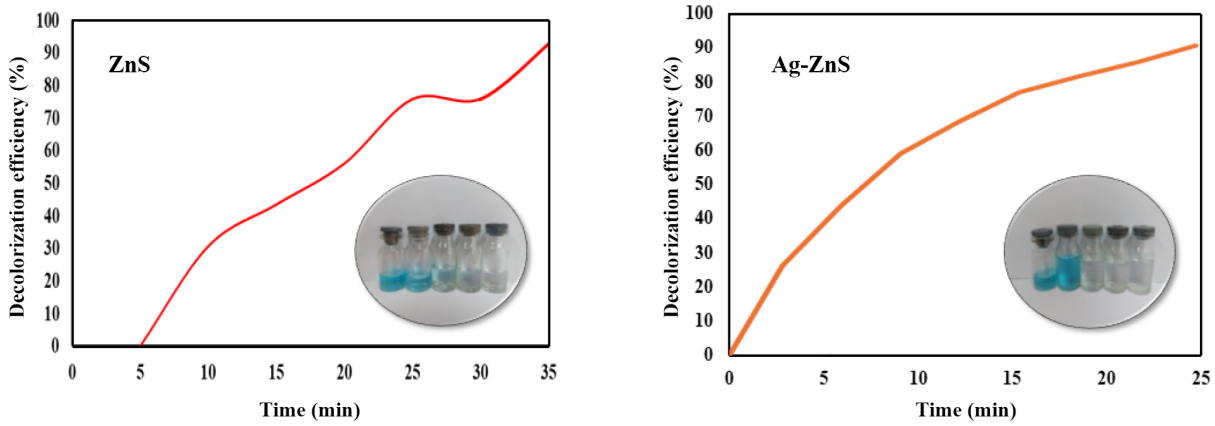

Fig. 7. Decolorization performance of the samples under UV light irradiation.

4. Conclusions

In conclusion, this research explored the impact of silver (Ag) on zinc sulfide (ZnS) semiconductors in facilitating the photocatalytic degradation of methylene blue under UV light exposure. The doped silver enhanced the photocatalytic activity compared to pure zinc sulfide (ZnS). Additionally, the Ag-ZnS sample made using the co-precipitation approach performed better than the other methods, as demonstrated by the photocatalytic findings. Lastly, under UV illumination, the Ag-ZnS photocatalyst that had been tuned could also efficiently break down methylene blue (MB) in aqueous pollutants. This research might lead to new avenues for enhancing ZnS-based nanoparticles' photocatalytic capabilities for the treatment of wastewater and water.

CRediT authorship contribution statement

Amir Hossein Afzal: Writing - original draft, Writing - review & editing, Conceptualization, Methodology, Formal Analysis, Data curation.
Arshia Seddiqi: Writing - original draft, Methodology, Conceptualization, Software.
Zahra Akbari: Writing - original draft, Methodology, Investigation, Formal Analysis.
Maryam Hajiebrahimi: Writing – original draft, Writing – review & editing, Data curation, Software, Visualization, Resources.
Sanaz Alamdari: Writing – review & editing, Investigation, Formal Analysis, Data curation, Validation.
Omid Mirzaee: Writing – review & editing, Visualization, Validation, Project administration, Supervision.

Data availability

The data underlying this article will be shared on reasonable request to the corresponding author.

Declaration of competing interest

The authors declare no competing interests.

Funding and acknowledgment

The authors wish to acknowledge Semnan University for all its support throughout this work.

References

[1] K. Faith Ngulube, A. Abdelhaleem, M. Fujii, M. Nasr, Synergism of Artificial Intelligence and Techno-Economic for Sustainable Treatment of Methylene Blue Dye-Containing Wastewater by Photocatalysis, Sustainability. 16 (2024) 529. https://doi.org/10.3390/su16020529.
[2] A. Gangadhar, A. Mavinakere Ramesh, J. Krishnegowda, S. Shivanna; Photo-catalytic dye degradation of methylene blue by using ZrO2/MWCNT nanocomposites, Water Pract. Technol. 16 (2021) 1265–1276. https://doi.org/10.2166/wpt.2021.066.
[3] F.-F. Zhang, Y. Han, Q. Liang, M. Wu, X. Wang, et al., Visible light-assisted photocatalytic degradation of methylene blue in water by highly chemically stable Cd-coordination polymers at room temperature, New J. Chem. 45 (2021) 19660–19665. https://doi.org/10.1039/D1NJ03958J.
[4] A. Chakrabarti, E. Alessandri, Syntheses, Properties, and Applications of ZnS-Based Nanomaterials, Appl. Nano. 5 (2024) 116–142. https://doi.org/10.3390/applnano5030010.
[5] P. Sehrawat, S.K. Mehta, S.K. Kansal, Synergistic enhancement of photocatalytic activity in ZnS/P-doped-MoS2 composite for hydrogen generation simultaneously oxidation of benzyl alcohol through water splitting and dye degradation, Int. J. Hydrog. Energy. 80 (2024) 573–585. https://doi.org/10.1016/j.ijhydene.2024.07.147.
[6] Y. Wang, F. Xu, L. Sun, Y. Li, L. Liao, et al., A highly active Z-scheme SnS/Zn2SnO4 photocatalyst fabricated for methylene blue degradation, RSC Adv. 12 (2022) 31985–31995. https://doi.org/10.1039/D2RA05519H.
[7] D.G. Ayu, S. Gea, Andriayani, D. Junita Telaumbanua, A.F. Rahman Piliang, et al., Photocatalytic degradation of methylene blue using N-doped ZnO/carbon dot (N-ZnO/CD) nanocomposites derived from organic soybean, ACS Omega. 8 (2023) 14965–14984. https://doi.org/10.1021/acsomega.2c07546.
[8] H. Moon, S. Kim, S.W. Joo, M. Kim, N.K. Park, et al., Design and selective photocatalytic activity of highly concentrated C, N, O co-doped Zn, S co-defective ZnS particles mediated by ethylenediamine derivatives, Nano Today. 49 (2023) 101785. https://doi.org/10.1016/j.nantod.2023.101785.
[9] A. Oskenbay, D. Salikhov, O. Rofman, I. Rakhimbek, Z. Shalabayev, et al., Solid-state synthesis of ZnS/ZnO nanocomposites and their

decoration with NiS cocatalyst for photocatalytic hydrogen production, Ceram. Int. 49 (2023) 32246–32260. https://doi.org/10.1016/j.ceramint.2023.07.200.

[10] L. Song, J. Hu, X. Lu, Z. Lu, J. Xie, et al., Boosting the photocatalytic activity and resistance of photostability of ZnS nanoparticles, Inorg. Chem. 61 (2022) 8217–8225. https://doi.org/10.1021/acs.inorgchem.2c00632.

[11] S. Alamdari, M. Haji Ebrahimi, O. Mirzaee, M. Jafar Tafreshi, M.H. Majlesara, et al., Cerium doped Tungsten-Based Compounds for Thermoluminescence Application, Prog. Phys. Appl. Mater. 2 (2022) 35–40. https://doi.org/10.22075/PPAM.2022.27086.1028.

[12] A. Balapure, J. Ray Dutta, R. Ganesan, Recent advances in semiconductor heterojunctions: a detailed review of the fundamentals of photocatalysis, charge transfer mechanism and materials, RSC Appl. Interfaces. 1 (2024) 43–69. https://doi.org/10.1039/D3LF00126A.

[13] B. Xiao, T. Lv, J. Zhao, Q. Rong, H. Zhang, et al., Synergistic effect of the surface vacancy defects for promoting photocatalytic stability and activity of ZnS nanoparticles, ACS Catal. 11 (2021) 13255–13265. https://doi.org/10.1021/acscatal.1c03476.

[14] L. Qin, S. Yang, D. Ding, J. Tan, J. Liu, R. Chen, Local-interaction-field-coupled semiconductor photocatalysis: recent progress and future challenges, J. Mater. Chem. A. 9 (2021) 2491–2525. https://doi.org/10.1039/D0TA09059J.

[15] N. Goodarzi, Z. Ashrafi-Peyman, E. Khani, A.Z. Moshfegh, Recent Progress on Semiconductor Heterogeneous Photocatalysts in Clean Energy Production and Environmental Remediation, Catalysts. 13 (2023) 1102. https://doi.org/10.3390/catal13071102.

[16] G.-J. Lee, J.J. Wu, Recent developments in ZnS photocatalysts from synthesis to photocatalytic applications—A review, Powder Technol. 318 (2017) 8–22. https://doi.org/10.1016/j.powtec.2017.05.022.

[17] M.M.H. Farahani, M. Hajiebrahimi, S. Alamdari, A. Najafzadehkhoee, G.M. Khounsaraki, et al., Synthesis and antibacterial activity of silver doped zinc sulfide/chitosan bionanocomposites: A new frontier in biomedical applications, Int. J. Biol. Macromol. 280 (2024) 135934. https://doi.org/10.1016/j.ijbiomac.2024.135934.

[18] Y. Yang, M. Toyoda, A. Yamaguchi, Y. Cho, A.N. El Aisnada, et al., Bandgap widening through doping for improving the photocatalytic oxidation ability of narrow-bandgap semiconductors, Phys. Chem. Chem. Phys. 25 (2023) 255–261. https://doi.org/10.1039/D2CP02994D.

[19] S. Patil, S. Jagadale, Co-precipitation methods for the synthesis of metal oxide nanostructures, Solution Methods for Metal Oxide Nanostructures, Elsevier. (2023) 39–60. https://doi.org/10.1016/B978-0-12-824353-4.00016-6.

[20] N. Kumari, S. Sareen, M. Verma, S. Sharma, A. Sharma, et al., Zirconia-based nanomaterials: recent developments in synthesis and applications, Nanoscale Adv. 4 (2022) 4210–4236. https://doi.org/10.1039/D2NA00367H.

[21] N. Baig, I. Kammakakam, W. Falath, Nanomaterials: A review of synthesis methods, properties, recent progress, and challenges, Mater. Adv. 2 (2021) 1821–1871. https://doi.org/10.1039/D0MA00807A.

[22] A. Rajaeiyan, M.M. Bagheri-Mohagheghi, Comparison of sol-gel and co-precipitation methods on the structural properties and phase transformation of γ and α-Al2O3 nanoparticles, Adv. Manuf. 1 (2013) 176–182. https://doi.org/10.1007/s40436-013-0018-1.

[23] X. Liu, Q. Liu, C. Chen, Ultrasonic oscillation synthesized ZnS nanoparticles/layered MXene sheet with outstanding photocatalytic activity under visible light, Vacuum. 183 (2021) 109834. https://doi.org/10.1016/j.vacuum.2020.109834.

[24] D.V. Markovskaya, A.V. Zhurenok, S.V. Cherepanova, E.A. Kozlova, Solid solutions of CdS and ZnS: Comparing photocatalytic activity and photocurrent generation, Appl. Surf. Sci. Adv. 4 (2021) 100076. https://doi.org/10.1016/j.apsadv.2021.100076.

[25] B. Poornaprakash, H. Park, K. Subramanyam, S.P. Vattikuti, K.C. Devarayapalli, et al., Doping-induced photocatalytic activity and hydrogen evolution of ZnS: V nanoparticles, Ceram. Int. 47 (2021) 26438–26446. https://doi.org/10.1016/j.ceramint.2021.06.055.

[26] J. Luciano-Velázquez, Y. Xin, Y.F. Su, C.I. Quiles-Vélez, S.A. Cruz-Romero, et al., Synthesis, characterization, and photocatalytic activity of ZnS and Mn-doped ZnS nanostructures, MRS Adv. 6 (2021) 252–258. https://doi.org/10.1557/s43580-021-00035-y.

[27] N. Dixit, J.V. Vaghasia, S.S. Soni, M. Sarkar, M. Chavda, et al., Photocatalytic activity of Fe doped ZnS nanoparticles and carrier mediated ferromagnetism, J. Environ. Chem. Eng. 3 (2015) 1691–1701. https://doi.org/10.1016/j.jece.2015.06.010.

[28] M. Jothibas, C. Manoharan, S. Johnson Jeyakumar, P. Praveen, I. Kartharinal Punithavathy, J. Prince Richard, Synthesis and enhanced photocatalytic property of Ni doped ZnS nanoparticles, Sol. Energy. 159 (2018) 434–443. https://doi.org/10.1016/j.solener.2017.10.055.

[29] H.R. Rajabi, M. Farsi, Effect of transition metal ion doping on the photocatalytic activity of ZnS quantum dots: synthesis, characterization, and application for dye decolorization, J. Mol. Catal. A: Chem. 399 (2015) 53–61. https://doi.org/10.1016/j.molcata.2015.01.029.

[30] M. Hajiebrahimi, S. Alamdari, O. Mirzaee, M. Tajally, Luminescence Investigation of Ce Doped ZnO/CdWO4 Nanocomposite, Adv. Ceram. Prog. 8 (2022) 8–12. https://doi.org/10.30501/acp.2022.363264.1102.

[31] X.M. Shuai, W.Z. Shen, A facile chemical conversion synthesis of ZnO/ZnS core/shell nanorods and diverse metal sulfide nanotubes, J. Phys. Chem. C. 115 (2011) 6415–6422. https://doi.org/10.1021/jp2005716.

[32] L. Li, T.J. Daou, I. Texier, T.T. Kim Chi, N.Q. Liem, P. Reiss, Highly luminescent CuInS2/ZnS core/shell nanocrystals: cadmium-free quantum dots for in vivo imaging, Chem. Mater. 21 (2009) 2422–2429. https://doi.org/10.1021/cm900103b.